

---

# Medical Vision Generalist: Unifying Medical Imaging Tasks in Context

---

Sucheng Ren<sup>1</sup> Xiaoke Huang<sup>2</sup> Xianhang Li<sup>2</sup> Junfei Xiao<sup>1</sup> Jieru Mei<sup>1</sup> Zeyu Wang<sup>2</sup>  
Alan Yuille<sup>1</sup> Yuyin Zhou<sup>2</sup>

<sup>1</sup>Johns Hopkins University

<sup>2</sup>UC Santa Cruz

## Abstract

This study presents Medical Vision Generalist (MVG), the first foundation model capable of handling various medical imaging tasks—such as cross-modal synthesis, image segmentation, denoising, and inpainting—within a unified image-to-image generation framework. Specifically, MVG employs an in-context generation strategy that standardizes the handling of inputs and outputs as images. By treating these tasks as an image generation process conditioned on prompt image-label pairs and input images, this approach enables a flexible unification of various tasks, even those spanning different modalities and datasets. To capitalize on both local and global context, we design a hybrid method combining masked image modeling with autoregressive training for conditional image generation. This hybrid approach yields the most robust performance across all involved medical imaging tasks. To rigorously evaluate MVG’s capabilities, we curated the first comprehensive generalist medical vision benchmark, comprising 13 datasets and spanning four imaging modalities (CT, MRI, X-ray, and micro-ultrasound). Our results consistently establish MVG’s superior performance, outperforming existing vision generalists, such as Painter and LVM. Furthermore, MVG exhibits strong scalability, with its performance demonstrably improving when trained on a more diverse set of tasks, and can be effectively adapted to unseen datasets with only minimal task-specific samples. The code is available at <https://github.com/OliverRensu/MVG>.

## 1 Introduction

The precise interpretation of medical images is imperative for timely disease detection, diagnosis, and treatment [1, 2]. Deep-learning based models have emerged as powerful tools in medical image analysis, tackling various challenges spanning from segmenting specific anatomical structures [3, 4, 5], localizing single organ diseases [6, 7, 8, 9, 10, 11, 12], to cross-modality image synthesis on brain MRI [13, 14, 15, 16]. However, these models, often referred to as specialist models, are typically customized for specific tasks, modalities, or anatomical regions. While this specialization often results in exceptional performance in certain contexts, it can lead to a severe performance drop when applied to new tasks or when tasked with training multi-domain data.

To address this challenge, recently, there has been a partial shift of research focus in developing generalist medical AI models [17, 18], which necessitate only a single training phase but are capable of wide application across a diverse array of medical tasks. Specifically, these generalist frameworks unify input and output spaces, allowing for straightforward adaptation to various tasks through the use of user-provided prompts. While existing generalist medical AI models like MedSAM have demonstrated impressive performance [19, 20, 21], their applicability in medical visual tasks remains limited. A unified, truly generalist vision model capable of addressing a vast array of medical imaging tasks remains a critical missing piece in the current medical research landscape.

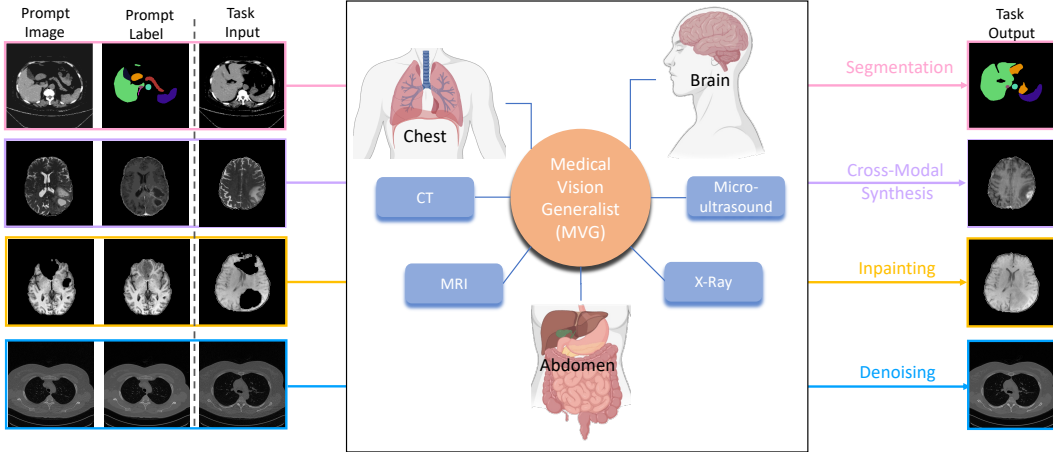


Figure 1: **Medical Vision Generalist** enables a single model be capable of performing **four** types of medical vision tasks on images in **four** medical imaging modalities of **three** major body regions.

Motivated by the remarkable success of in-context learning in natural language processing [22, 23] and computer vision [24, 25, 26], we hereby propose Medical Vision Generalist (MVG), the **first** generalist model in the medical imaging domain. Specifically, MVG leverages an in-context learning framework to unify a set of medical imaging tasks, including cross-modal synthesis, denoising, segmentation, and inpainting across modalities like CT, MRI, X-ray, and Micro-ultrasound. In contrast to prior task- and data-specific medical AI models, MVG offers adaptability to new data with minimal labeled samples, eliminating the need for retraining. To achieve this, MVG first standardizes the input/output space using in-context coloring, which maps various tasks into a single-channel coloring scheme. This removes the need for task-specific heads, thus regulating the model to learn exclusively from prompts. Subsequently, tasks are unified through conditional image generation, where MVG generates output conditioned on both the task prompt and a sample image.

To capture both local and global context, we devise a hybrid strategy that combines masked image modeling and autoregressive training for conditional image generation. The former involves concatenating prompt images, labels, task inputs, and labels, followed by random masking; the latter constructs prompt image-label pairs, task inputs, and labels as long visual sentences. During inference, MVG conditions predictions on the prompts selected from locations closely matching the task images, ensuring contextual relevance and guidance that enhances output quality and consistency.

Furthermore, we have curated the first unified medical imaging benchmark, encompassing 13 datasets spanning a range of human anatomies (e.g., abdomen, pelvis, brain, chest) and modalities (e.g., CT, MRI, X-ray, micro-ultrasound). This new benchmark enables a comprehensive assessment of our MVG models. Experimental results demonstrate the effectiveness of our medical vision generalist in performing various medical vision tasks with only one model. As illustrated in Figure 2, our medical vision generalist outperforms the previous generalist models by a large margin. For instance, our MVG achieves 0.735 mIoU on all segmentation tasks and outperforms the previous best vision generalist by 0.123 mIoU. Furthermore, our MVG demonstrates two intriguing properties: 1) it scales well with multiple tasks and datasets, suggesting its potential to excel further as diverse datasets continue to emerge; and 2) it can efficiently generalize to new datasets, with only a few specific examples needed for each task.

## 2 Related Work

**Medical Image Analysis.** In the field of medical image analysis, there have been key developments in deep-learning models for image segmentation. As the earliest success in this line of work, U-Net [27] uses an encoder-decoder architecture with skip-connection, revealing the great potential of deep networks. Following the line, nnUnet [28] further improves the model architecture and introduces bags of tricks, building a well-engineered general segmentation model. TransUnet [29] proposed to use pre-trained ViT for better feature extraction. Recent efforts in medical image analysis have produced remarkable models capable of performing a variety of tasks. Notable works include "One

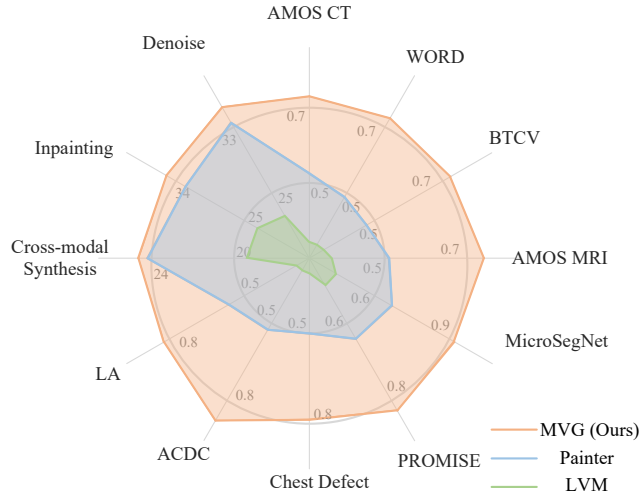


Figure 2: **Comparison with other generalists.** Our model achieves state-of-the-art performance on all involved medical vision tasks of five types.

model to rule them all" [30], MedSAM [19], and UniverSeg [21], which are designed to tackle unified medical segmentation tasks. UniverSeg adapts UNet [27] to intake in-context samples to segment new data and tasks without further training. Besides, biomedGPT [20] proposes a unified generative model for bio-medical vision-language tasks. In this paper, we propose a novel paradigm to build a generalist model, which is capable of handling various medical vision tasks, including segmentation, inpainting, cross-modal synthesis, and denoising.

**Universal Models and In-Context Learning.** The advent of the universal Transformer architecture and its success in generative pretraining has inspired the development of universal models that tackle a wide range of computer vision tasks [31, 32, 33, 34, 24, 26]. In-context learning is a novel few-shot learning paradigm that emerged in large language models and was first proposed by GPT-3 [35]. Specifically, in-context learning enables one model to perform different tasks with only in-context examples as prompts. While the prompts for language models are mostly defined as a few sentences, in-context learning in other domains is still in an early exploration stage. As one of the earliest works, Flamingo [36] extends the modality of in-context learning with language instructions and sequences of images and videos. Perceiver-IO [37] uses the Transformer architecture for a general-purpose model that handles data from arbitrary settings like natural language, visual understanding, multi-modal reasoning, and StarCraft II. AD [38] introduces in-context learning to reinforcement learning with algorithm distillation. DPT [39] provides a sample-efficient RL algorithm with strong in-context decision-making. In this paper, we use a sequence of paired medical images to build a vision model with in-context learning ability, unifying 13 medical tasks as a generation task.

### 3 Method

Unlike previous medical AI models, which are specific to one or a few predefined imaging tasks and produce a predetermined set of outputs, the proposed MVG aims to offer unprecedented flexibility across tasks, modalities, and datasets. The key idea is to unify medical imaging tasks, such as cross-modal synthesis, image segmentation, denoising, and inpainting, within an image-to-image generation framework.

#### 3.1 Tasks

Our Medical Vision Generalist (MVG) is designed to address various medical imaging tasks, with a particular emphasis in this study on segmentation, cross-modal synthesis, inpainting, and denoising, tasks for which well-represented public datasets are available. However, it is crucial to note that its design should be widely applicable to any image-to-image generation task.

**Segmentation.** Medical image segmentation, including CT, MRI, X-ray, and Micro-ultrasound segmentation, involves dividing an image obtained from these modalities into distinct segments to

isolate regions of interest, such as organs or abnormalities. The input space for these tasks typically consists of images from CT, MRI, X-ray, or Micro-ultrasound scans. The output space is represented by a mask, where each value (excluding the background) in the mask corresponds to a different class or type of object, such as a liver or kidney.

**Cross-modal synthesis.** Cross-modal synthesis aims to generate images in one modality from images of another modality for the same subject, aiding in visualization and facilitating multi-modal medical image analysis. The input space and output space are different medical imaging modalities.

**Brain image inpainting.** In the context of brain image processing, inpainting refers to the process of synthesizing healthy brain tissue in regions affected by glioma, a type of brain tumor [40]. Inpainting allows professionals to effectively utilize non-standard imaging protocols and directly apply brain parcellation tools to facilitate treatment planning. The input space is the corrupted brain MRI and the output space is the corresponding brain MRI restoring the affected regions to a normal state.

**Denoising.** Denoising aims to reconstruct full-dose CT images from low-dose CT images, allowing for reduced radiation doses during CT scans while preserving diagnostic image quality. The input space is the scanned CT image with low-dose radiation, while the output space is the corresponding image with full-dose radiation.

### 3.2 Unifying the Input/Output Space

Assume an input image is denoted as  $\mathbf{x} \in \mathcal{R}^{H \times W}$ , the output could be a segmentation map, a synthesized brain image in the target modality, a restored normal brain MRI or a full-dose CT image of the same size. To unify the output space of images across tasks, our MVG adopts a strategy beyond task-specific heads: mapping different tasks into a single-channel coloring scheme, inspired by [26, 25]. We explore three different in-context coloring methods that circumvent reliance on label values, including binary, pre-defined, and random colorization, as detailed below.

**Binary colorization.** We break down the problem of segmenting multiple classes into individual binary segmentation tasks, each focusing on separating one class from the background. Specifically, if a segmentation mask contains  $N_k$  foreground classes, we simply split it to  $N_k$  binary masks. However, this requires multiple inferences when an image contains more than one foreground class.

**Pre-defined colorization.** In this approach, we allocate a predetermined unique color to each segmentation mask derived from diverse datasets. Suppose there are  $K$  segmentation datasets, with each dataset containing  $N_k$  classes. Consequently, the  $n_{th}$  class of the  $k_{th}$  dataset is assigned the value of  $\sum_{i=1}^{k-1} i * N_i + n$ . Note that different tasks may involve classes with identical semantics; for example, both the AMOS segmentation dataset [3] and the Synapse dataset [41] include the class "Liver". However, distinct colors are assigned to the same class across different tasks.

**Random colorization.** The use of pre-defined colors may restrict the adaptability and efficacy of medical vision generalists, as they can cause the model to focus on learning tasks based on the color of the prompt rather than the contextual information [25]. To address this limitation, we build a set of colors and randomly sample colors for different semantics in one iteration but the same semantic in the prompt label and task label share the same color.

Except for medical image segmentation, the outputs of all other tasks in this study do not involve categorical values that need to be predicted. Therefore, we do not apply coloring for these tasks.

### 3.3 Task Unification via Conditional Image Generation

After standardizing the input and output space for all tasks as images of identical sizes, we construct the training input, including 1) the task prompt consisting of paired prompt images and prompt labels, and 2) the task input and its associated label. We then unify various medical imaging tasks within a conditional image-to-image generation framework using the task prompt as task specification. All the tasks are unified to generate the task label  $Y \in \mathcal{R}^{\tilde{H} \times \tilde{W}}$  based on the condition including the task image  $X \in \mathcal{R}^{H \times W}$ , the prompt image  $P_x \in \mathcal{R}^{H \times W}$ , and the prompt label  $P_y \in \mathcal{R}^{\tilde{H} \times \tilde{W}}$ . Specifically, we use two conditional image generation frameworks - mask image modeling [42] and autoregressive training [43].

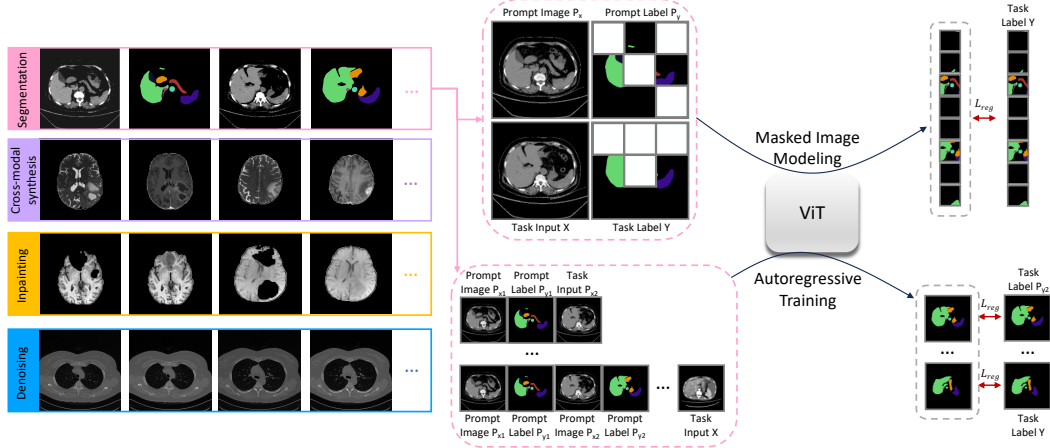


Figure 3: **Method overview.** **Left:** Four types of medical tasks (*i.e.*, segmentation, cross-modal synthesis, inpainting, and denoising) are unified as a universal image-to-image generation task with in-context learning. **Right:** We adopt mask image modeling and auto-regressive training for in-context generation.

**Architecture Selection.** Following the same setting in [42, 44], we take vanilla ViT [45] as an encoder including a patch embedding layer and several Transformer blocks. The decoder is a simple prediction head with two convolution layers and takes four feature maps [46] from ViT as input.

**Mask Image Modeling.** During training, we form a square image by concatenating the prompt image (upper left) with its corresponding label (upper right), as well as the task image (lower left) with its associated label (lower right), as illustrated in Figure 3(a). We perform random masking on the square image and train ViT to reconstruct the masked region [26]:

$$p(x) = \prod_{i=1}^M p(x_i | x_{x \notin x_M}, \theta). \quad (1)$$

where  $x_M$  is the mask region,  $x_{x \notin x_M}$  is the visible region, and  $\theta$  denotes the model parameters. However, in practice, we observed that mask image modeling yields unsatisfactory results for medical image segmentation. We hypothesize that this may be attributed to the masking strategy’s potential to compromise the preservation of global contextual information and to ignore small regions-of-interest. To ensure the efficacy on medical image segmentation, we introduce an additional *auto-regressive* training, which preserves the global context within individual images, as shown below.

**Auto-Regressive Training.** In auto-regressive training, each image, including paired prompt images, prompt labels, task inputs, and associated labels, is treated as a single element in a sequential data structure. The model is fed with a partial sequence and trained to predict the next image in the sequence conditioning on the preceding ones.

Mathematically, let  $P_{x_1}, P_{y_1}, \dots, P_{x_n}, P_{y_n}, X, Y$  denote  $n + 1$  pairs of images and labels. The first  $n$  pairs serve as the task prompt, and the model learns to predict the task output  $Y$  given the task input  $X$  and the prompt. This process iterates through each pair in the sequence. For each iteration, auto-regressive training is conducted with supervision solely on prompt labels and the task label:

$$S = [S_1, S_2, \dots, S_{2n-1}, S_{2n}, S_{2n+1}, S_{2n+2}] = [P_{x_1}, P_{y_1}, \dots, P_{x_n}, P_{y_n}, X, Y],$$

$$p(x) = \prod_{i=1}^{n+1} p(S_{2i} | S_1, \dots, S_{2i-1}, \theta). \quad (2)$$

**Loss Function.** Any regression loss function like  $l_1$  or  $l_2$  can serve as the loss function of our MVG. Different from the  $l_2$  loss function in MAE [42], we find the smooth  $l_1$  performs best for MVG.

**Inference.** We first construct a sequence  $S = [P_x, P_y, X, \hat{Y}]$ , where prompts, the task image, and the desired output are concatenated together. MVG leverages the task prompt, composed of the prompt

Region	Dataset	Modality	#Training	#Testing	Task
Abdomen	AMOS [3]	CT	240	120	Segmentation
Abdomen	WORD [4]	CT	100	20	Segmentation
Abdomen	BTCV [47]	CT	21	9	Segmentation
Abdomen	AMOS [3]	MRI	60	50	Segmentation
Pelvis	MicroSegNet [48]	Micro-US	55	20	Segmentation
Pelvis	PROMISE [49]	MRI	50	30	Segmentation
Brain	BraTS-GLI [50]	MRI	1251	219	Cross-modal synthesis
Brain	BraTS-Local [50]	MRI	1000	251	Inpainting
Chest	Low dose [51]	CT	200	59	Denosing
Chest	Defect Detection [52]	Xray	15	6	Segmentation
Chest	ACDC [53]	MRI	100	50	Segmentation
Chest	LA [54]	MRI	81	20	Segmentation

Table 1: **Datasets overview.** Our MVG is trained and evaluated on 13 different datasets covering four major human body regions (*i.e.*, Abdomen, Pelvis, Brain, Chest). #Training/Testing refers to the number of samples for training and testing.

image  $P_x$  and label  $P_y$ , for task specification, subsequently generating predictions by conditioning on both the task input  $X$  and the task prompt. Since the task prompt is formulated as images, MVG demonstrates versatility in defining imaging tasks, capable of handling data sourced from diverse scanning machines, procedures, settings, or populations. For instance, if  $P_x$  and  $P_y$  represent an image and label extracted from the AMOS CT training set, respectively, MVG performs multi-organ segmentation on the image  $X$  derived from the AMOS CT testing set, maintaining consistency within the dataset setting and guided by the provided context.

Different task prompts can yield varying results. In this study, we address this variability by selecting the prompt image from a location that closely matches the task image. Given the instance  $X_{TE}$  which has  $N_{TE}$  slices from the testing set, we randomly choose an instance  $X_{TR}$  which has  $N_{TR}$  slices and the corresponding label  $Y_{TR}$  from the training set. For the  $n_{th}$  slice of  $X_{TE}$ , we also choose the the floor( $\frac{n_{th} * N_{TR}}{N_{TE}}$ ) slice as the prompt.

## 4 Experiment

### 4.1 Implementation Details

**Data.** As shown in Table 1, our model is developed on 13 different datasets covering four major human body regions (*i.e.*, Abdomen, Pelvis, Brain, Chest). More details can be found in the appendix. Following the standard preprocessing strategy, we apply a windowing range of [-100, 200] to all involved CT scans for better contrast. Input images are firstly resized to  $512 \times 512$  and then randomly cropped with a size of  $448 \times 448$ . To evaluate the generalization of MVG, we choose MSD [55], a multi-organ segmentation dataset as an out-of-distribution dataset.

**Training details.** AdamW optimizer is used with a weight decay of 0.05. The peak learning is set to  $1e^{-3}$  with a cosine learning rate scheduler. We train our model 100 epochs with 5 warm-up epochs. We only adopt the random crop as the data augmentation. The sampling weight of segmentation tasks is 0.5 while the rest of the tasks share 0.5. We use 8 A5000 GPUs to train our models. We use 1 in-context sample for both training and inference.

**Training Objective.** In practice, for *all tasks except segmentation*, we perform 90% training iteration with *mask image modeling* and 10% training iteration with *auto-regressive* training. For *segmentation* tasks, we perform 100% training iterations with *auto-regressive* training.

**Evaluation.** We use mean IoU (mIoU) as the evaluation metric for segmentation. For cross-modal synthesis, inpainting, and denosing, we use mean absolute error (MAE), peak signal-to-noise ratio (PSNR), and structural similarity index measure (SSIM) as the evaluation metric.

### 4.2 A Generalist to 13 Medical Tasks

**Baselines.** Our generalist baselines includes LVM [24] and Painter [26], which are trained on our benchmark. UniverSeg [21] is used as a segmentation generalist baseline. While our specialist base-

Method	AMOS CT	WORD	BTCV	AMOS MRI	MicroSegNet	PROMISE	Chest Defect	ACDC	LA
<i>Specialists</i>									
ResNet-18	0.55	0.50	0.51	0.53	0.67	0.75	0.62	0.69	0.68
UNet	0.81	0.83	0.82	0.81	0.90	0.91	0.89	0.86	0.83
VNet	0.70	0.75	0.72	0.73	0.90	0.89	0.86	0.87	0.84
TranUNet	0.80	0.82	0.84	0.82	0.94	0.90	0.88	0.88	0.84
nnUNet	0.87	0.90	0.91	0.88	0.97	0.93	0.90	0.90	0.89
<i>Generalists</i>									
UniverSeg*	0.20	0.29	0.37	0.25	0.71	0.55	0.55	0.54	0.57
Painter	0.52	0.48	0.45	0.51	0.69	0.68	0.50	0.52	0.55
LVM	0.12	0.14	0.10	0.15	0.36	0.30	0.10	0.12	0.13
MVG	0.73	0.74	0.73	0.74	0.91	0.85	0.79	0.85	0.81

Table 2: **Quantitative evaluation in segmentation tasks.** Compared to other generalists, our method achieves state-of-the-art performance with solid improvements. \*: We inference the official weights with the 64 in-context samples from training set.

Method	Cross-modal synthesis			Inpainting			Denoise		
	MAE	PSNR	SSIM	MAE	PSNR	SSIM	MAE	PSNR	SSIM
<i>Specialists</i>									
ResNet-18	0.026	20.984	0.860	0.008	30.981	0.959	0.022	30.519	0.709
Pix2Pix	0.018	24.311	0.899	0.008	34.891	0.982	0.020	33.011	0.730
TranUNet	0.016	25.541	0.938	0.005	35.561	0.989	0.016	33.999	0.761
<i>Generalists</i>									
Painter	0.021	24.031	0.920	0.006	33.595	0.978	0.020	33.104	0.721
MVG	0.019	24.721	0.929	0.006	34.521	0.981	0.018	33.521	0.731

Table 3: **Quantitative comparison with other tasks.** Our model shows strong capabilities in the tasks of cross-modal synthesis, inpainting, and denoising.

lines includes ResNet-18 [56] with a two-layer MLP decoder, UNet [27], VNet [57], TransUNet [29], and nnUNet [28]. For synthesis tasks, we involve Pix2Pix [58] as an additional baseline.

**Quantitative evaluation.** In Table 2, we compare our method with the latest vision generalist models [24, 26] across a range of segmentation tasks. Our medical vision generalist achieves the best performance of 0.79 mIoU among all the generalists. Specifically, Our medical vision generalist outperforms Painter [26] by 0.24 mIoU, LVM [24] by 0.62 mIoU on average, and UniverSeg [21] by 0.35 mIoU. All the generalists only require one model to perform these different tasks. UniverSeg is trained with up to 64 in-context samples, yet still yields inferior performance to our method which only relies on 1 in-context sample. At the same time, specialist models like UNet [27], TranUNet [29], and nnUNet [28], which need to train different models for different tasks, still hold the edge in performance.

We report the image synthesis results in Table 3. we present a detailed quantitative comparison of our method with the latest generalist and specialist models across various tasks including cross-modal synthesis, inpainting, and denoising. Our Medical Vision Generalist (MVG) model demonstrates strong capabilities and achieves competitive performance, particularly in the generalist category. For instance, in the task of cross-modal synthesis, MVG shows an improvement over Painter in all metrics: a lower Mean Absolute Error (MAE) by 0.002, a higher Peak Signal-to-Noise Ratio (PSNR) by 0.69, and a better Structural Similarity Index (SSIM) by 0.009 over the best vision generalist.

**Qualitative evaluation.** To provide a more intuitive observation of our medical vision generalist, we provide the visualization of different tasks in Figure 4.

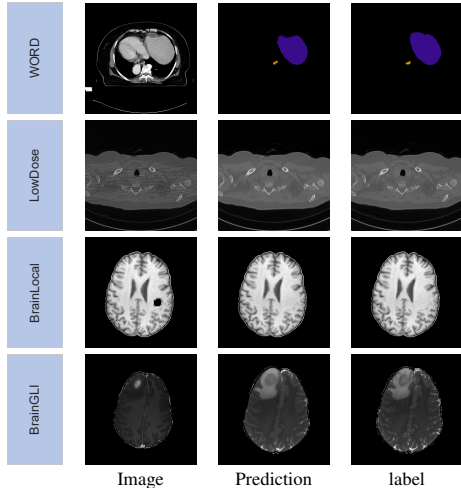


Figure 4: **Qualitative evaluation of four tasks:** Segmentation (1st row), denoising (2nd row), cross-modal synthesis (3th row), and inpainting (4th row).

**Generalize to unseen datasets.** The advantage of in-context learning is that it allows models to adapt to new datasets quickly. We report the result in Table 4, MVG achieves 0.84 mIoU on MSD-Liver with only new prompts without any fine-tuning. After fine-tuning MVG with one instance on MSD-Spleen and MSD-Lung, MVG achieves 0.87 mIoU and 0.48 mIoU.

### 4.3 Ablation Study

**Data scalability.** Nowadays, more and more datasets are available, which motivates us to study whether a scale-up dataset can train a stronger medical vision generalist. As shown in Table 5, we randomly choose 1%, 10%, 50% as comparison with the **full data**. The performance of our medical vision generalist consistently improves with the growth of dataset size. These results show the strong dataset scalability of our medical vision generalist. We also compare it with the specialists, which are trained on each dataset separately, with the same data sampling proportion (*i.e.*, 1%, 10%, 50%). We can interpret that in the low data regime, the specialists suffer from overfitting.

**Color space.** To unify the output space of different segmentation tasks in which the same value from different datasets may have different semantics, we propose to unify the output space with a pre-defined color for each class or random color that we keep the same semantics have the colors. As shown in Table 5, the random color performs much better than the pre-defined color on abdominal segmentation while having a similar performance on prostate segmentation. In particular, our medical vision generalist with random color space gains the average result of 0.735 mIoU on abdominal segmentation and improves 0.123 mIoU over that with pre-defined color space. In contrast, our medical vision generalist achieves inferior performance with pre-defined or random colors. The random color makes medical vision generalists learn more from the context instead of the color itself and avoid the model being limited by the number of colors.

**Isolated and Unified training.** To prove our medical vision generalist can benefit from large-scale datasets across different tasks. We compare two settings: 1) isolated training: we train different models on different datasets in isolation. Namely, we train 13 models for the 13 datasets. 2) unified training: we train our medical vision generalist on all datasets together. Note that both settings have the same model architecture. We report the results in Table 5. The unified model makes significant improvements over the isolated model in all tasks and the improvements reach 0.14 mIoU. Such results indicate that the medical vision generalist can benefit from large-scale datasets even if this

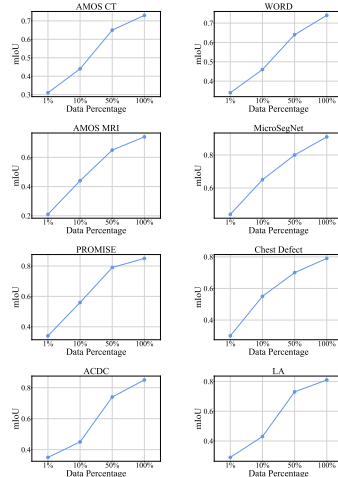


Figure 5: **Impact of training data scale.** We ablate on various scales of the training data (randomly sampled from each dataset), ranging from 1% to 100%.

Dataset	mIoU
MSD-Liver	0.84
MSD-Spleen	0.87
MSD-Lung	0.48

Table 4: Generalization to the unseen MSD dataset.

Method	AMOS CT	WORD	BTCV	AMOS MRI	MicroSegNet	PROMISE	Chest Defect	ACDC	LA
<i>a) Color Space</i>									
Binary	0.46	0.48	0.48	0.49	0.78	0.78	0.45	0.49	0.52
Pre-defined	0.60	0.62	0.62	0.61	0.89	0.86	0.71	0.74	0.73
Random	0.73	0.74	0.73	0.74	0.91	0.85	0.79	0.85	0.81
<i>b) Isolated vs. Unified Training</i>									
Isolated	0.55	0.57	0.57	0.58	0.80	0.77	0.70	0.69	0.68
Unified	0.73	0.74	0.73	0.74	0.91	0.85	0.79	0.85	0.81
<i>c) Auto-regressive vs. MIM in Segmentation Training</i>									
MIM (mask 50%)	0.56	0.48	0.46	0.54	0.70	0.66	0.50	0.50	0.52
MIM (mask 75%)	0.53	0.42	0.44	0.52	0.70	0.63	0.48	0.50	0.51
Auto-regressive	0.73	0.74	0.73	0.74	0.91	0.85	0.79	0.85	0.81

Table 5: **Ablation study:** *a) Color space for segmentation.* Using semantic masks in a random color space as prompts significantly improves the segmentation performance of our generalist model.

dataset has different annotation semantics which motivates the medical image analysis community to further expand the datasets.

**Auto-regressive vs. MIM.** We ablate the conditional image generation method: mask image modeling and auto-regressive training. As shown in Table 5, Auto-regressive training emerges as the significantly superior method, outperforming MIM across all datasets. The results underscore the fundamental weakness of random masking strategies in segmentation tasks, especially when dealing with small anatomical organs. By leveraging medical images’ inherent spatial and contextual information, auto-regressive training offers a powerful alternative that significantly enhances in-context learning and segmentation performance.

## 5 Conclusion and Discussion

**Conclusion.** In this work, we present MVG, a versatile model capable of handling various medical imaging tasks, including cross-modal synthesis, segmentation, denoising, and inpainting, within a unified image-to-image generation framework. MVG employs an in-context generation strategy to standardize inputs and outputs as images, allowing flexible task unification across various modalities and datasets. A hybrid approach combining masked image modeling and autoregressive training proved the most effective. To thoroughly assess MVG’s potential and limitations, we also curate the first comprehensive generalist medical vision benchmark consisting of 13 datasets across 4 imaging modalities, including CT, MRI, X-ray, and Micro-ultrasound. Experiment results demonstrate that MVG consistently outperforms existing vision generalists. Benefiting from the in-context learning scheme, MVG demonstrates exceptional flexibility, scalability and potential for generalization to unseen datasets with minimal samples. We will make our code and benchmark publicly available to encourage future research in medical AI generalists.

**Limitations.** Despite the encouraging results above, our MVG still falls behind the specialist models on different benchmarks. Additionally, the quality of MVG’s final prediction is sensitive to the choice of the in-context sample. We conjecture this is because, currently, we only use one in-context sample for both training and inference (due to computing resource constraints), but for the next step, we plan to explore techniques such as strategically selecting in-context samples to alleviate the problem. Our current framework is in 2D but in the future we plan to extend our method to 2.5D or 3D models.

### Acknowledge

This work is partially supported TPU Research Cloud (TRC) program, Google Cloud Research Credits program, and AWS Cloud Credit for Research program.

### References

- [1] Junlong Cheng, Shengwei Tian, Long Yu, Chengrui Gao, Xiaojing Kang, Xiang Ma, Weidong Wu, Shijia Liu, and Hongchun Lu. Resganet: Residual group attention network for medical image classification and segmentation. *Medical Image Analysis*, 76:102313, 2022.

- [2] Jeffrey De Fauw, Joseph R Ledsam, Bernardino Romera-Paredes, Stanislav Nikolov, Nenad Tomasev, Sam Blackwell, Harry Askham, Xavier Glorot, Brendan O’Donoghue, Daniel Visentin, et al. Clinically applicable deep learning for diagnosis and referral in retinal disease. *Nature medicine*, 24(9):1342–1350, 2018.
- [3] Yuanfeng Ji, Haotian Bai, Chongjian Ge, Jie Yang, Ye Zhu, Ruimao Zhang, Zhen Li, Lingyan Zhanng, Wanling Ma, Xiang Wan, et al. Amos: A large-scale abdominal multi-organ benchmark for versatile medical image segmentation. *Advances in Neural Information Processing Systems*, 35:36722–36732, 2022.
- [4] Xiangde Luo, Wenjun Liao, Jianghong Xiao, Jieneng Chen, Tao Song, Xiaofan Zhang, Kang Li, Dimitris N Metaxas, Guotai Wang, and Shaoting Zhang. Word: A large scale dataset, benchmark and clinical applicable study for abdominal organ segmentation from ct image. *arXiv preprint arXiv:2111.02403*, 2021.
- [5] Yabo Fu, Yang Lei, Tonghe Wang, Walter J Curran, Tian Liu, and Xiaofeng Yang. A review of deep learning based methods for medical image multi-organ segmentation. *Physica Medica*, 85:107–122, 2021.
- [6] Zhuotun Zhu, Yingda Xia, Lingxi Xie, Elliot K Fishman, and Alan L Yuille. Multi-scale coarse-to-fine segmentation for screening pancreatic ductal adenocarcinoma. In *International Conference on Medical Image Computing and Computer-Assisted Intervention*, pages 3–12. Springer, 2019.
- [7] Tianyi Zhao, Kai Cao, Jiawen Yao, Isabella Noguees, Le Lu, Lingyun Huang, Jing Xiao, Zhaozheng Yin, and Ling Zhang. 3d graph anatomy geometry-integrated network for pancreatic mass segmentation, diagnosis, and quantitative patient management. In *Proceedings of the IEEE/CVF Conference on Computer Vision and Pattern Recognition*, pages 13743–13752, 2021.
- [8] Yuankai Huo, Jinzheng Cai, Chi-Tung Cheng, Ashwin Raju, Ke Yan, Bennett A Landman, Jing Xiao, Le Lu, Chien-Hung Liao, and Adam P Harrison. Harvesting, detecting, and characterizing liver lesions from large-scale multi-phase CT data via deep dynamic texture learning. *arXiv preprint arXiv:2006.15691*, 2020.
- [9] Chi-Tung Cheng, Jinzheng Cai, Wei Teng, Youjing Zheng, Yu-Ting Huang, Yu-Chao Wang, Chien-Wei Peng, Youbao Tang, Wei-Chen Lee, Ta-Sen Yeh, et al. A flexible three-dimensional heterophase computed tomography hepatocellular carcinoma detection algorithm for generalizable and practical screening. *Hepatology Communications*, 2022.
- [10] Diego Ardila, Atilla P Kiraly, Sujeeth Bharadwaj, Bokyung Choi, Joshua J Reicher, Lily Peng, Daniel Tse, Mozziyar Etemadi, Wenxing Ye, Greg Corrado, et al. End-to-end lung cancer screening with three-dimensional deep learning on low-dose chest computed tomography. *Nature Medicine*, 25(6):954–961, 2019.
- [11] Roger Y Kim, Jason L Oke, Lyndsey C Pickup, Reginald F Munden, Travis L Dotson, Christina R Bellinger, Avi Cohen, Michael J Simoff, Pierre P Massion, Claire Filippini, et al. Artificial intelligence tool for assessment of indeterminate pulmonary nodules detected with CT. *Radiology*, page 212182, 2022.
- [12] Nicholas Heller, Fabian Isensee, Klaus H Maier-Hein, Xiaoshuai Hou, Chunmei Xie, Fengyi Li, Yang Nan, Guangrui Mu, Zhiyong Lin, Miofei Han, et al. The state of the art in kidney and kidney tumor segmentation in contrast-enhanced ct imaging: Results of the kits19 challenge. *Medical Image Analysis*, 67:101821, 2021.
- [13] Guoyang Xie, Yawen Huang, Jinbao Wang, Jiayi Lyu, Feng Zheng, Yefeng Zheng, and Yaochu Jin. Cross-modality neuroimage synthesis: A survey. *ACM computing surveys*, 56(3):1–28, 2023.
- [14] Hongwei Bran Li, Gian Marco Conte, Syed Muhammad Anwar, Florian Kofler, Ivan Ezhov, Koen van Leemput, Marie Piraud, Maria Diaz, Byrone Cole, Evan Calabrese, et al. The brain tumor segmentation (brats) challenge 2023: Brain mr image synthesis for tumor segmentation (brasyn). *ArXiv*, 2023.
- [15] Sanuwani Dayarathna, Kh Tohidul Islam, Sergio Uribe, Guang Yang, Munawar Hayat, and Zhaolin Chen. Deep learning based synthesis of mri, ct and pet: Review and analysis. *Medical Image Analysis*, page 103046, 2023.

- [16] Lingting Zhu, Zeyue Xue, Zhenchao Jin, Xian Liu, Jingzhen He, Ziwei Liu, and Lequan Yu. Make-a-volume: Leveraging latent diffusion models for cross-modality 3d brain mri synthesis. In *International Conference on Medical Image Computing and Computer-Assisted Intervention*, pages 592–601. Springer, 2023.
- [17] Michael Moor, Oishi Banerjee, Zahra Shakeri Hossein Abad, Harlan M Krumholz, Jure Leskovec, Eric J Topol, and Pranav Rajpurkar. Foundation models for generalist medical artificial intelligence. *Nature*, 616(7956):259–265, 2023.
- [18] Tao Tu, Shekoofeh Azizi, Danny Driess, Mike Schaekermann, Mohamed Amin, Pi-Chuan Chang, Andrew Carroll, Chuck Lau, Ryutaro Tanno, Ira Ktena, et al. Towards generalist biomedical ai. *arXiv preprint arXiv:2307.14334*, 2023.
- [19] Jun Ma, Yuting He, Feifei Li, Lin Han, Chenyu You, and Bo Wang. Segment anything in medical images. *Nature Communications*, 15(1):654, 2024.
- [20] Kai Zhang, Jun Yu, Zhiling Yan, Yixin Liu, Eashan Adhikarla, Sunyang Fu, Xun Chen, Chen Chen, Yuyin Zhou, Xiang Li, et al. Biomedgpt: A unified and generalist biomedical generative pre-trained transformer for vision, language, and multimodal tasks. *arXiv preprint arXiv:2305.17100*, 2023.
- [21] Victor Ion Butoi, Jose Javier Gonzalez Ortiz, Tianyu Ma, Mert R Sabuncu, John Guttag, and Adrian V Dalca. Universeg: Universal medical image segmentation. In *Proceedings of the IEEE/CVF International Conference on Computer Vision*, pages 21438–21451, 2023.
- [22] Tom B. Brown, Benjamin Mann, Nick Ryder, Melanie Subbiah, Jared Kaplan, Prafulla Dhariwal, Arvind Neelakantan, Pranav Shyam, Girish Sastry, Amanda Askell, Sandhini Agarwal, Ariel Herbert-Voss, Gretchen Krueger, T. J. Henighan, Rewon Child, Aditya Ramesh, Daniel M. Ziegler, Jeff Wu, Clemens Winter, Christopher Hesse, Mark Chen, Eric Sigler, Mateusz Litwin, Scott Gray, Benjamin Chess, Jack Clark, Christopher Berner, Sam McCandlish, Alec Radford, Ilya Sutskever, and Dario Amodei. Language models are few-shot learners. *ArXiv*, abs/2005.14165, 2020.
- [23] OpenAI. Gpt-4 technical report. *ArXiv*, abs/2303.08774, 2023.
- [24] Yutong Bai, Xinyang Geng, Karttikeya Mangalam, Amir Bar, Alan Yuille, Trevor Darrell, Jitendra Malik, and Alexei A Efros. Sequential modeling enables scalable learning for large vision models. *arXiv preprint arXiv:2312.00785*, 2023.
- [25] Xinlong Wang, Xiaosong Zhang, Yue Cao, Wen Wang, Chunhua Shen, and Tiejun Huang. Seggpt: Segmenting everything in context. *arXiv preprint arXiv:2304.03284*, 2023.
- [26] Xinlong Wang, Wen Wang, Yue Cao, Chunhua Shen, and Tiejun Huang. Images speak in images: A generalist painter for in-context visual learning. In *Proceedings of the IEEE/CVF Conference on Computer Vision and Pattern Recognition*, pages 6830–6839, 2023.
- [27] Olaf Ronneberger, Philipp Fischer, and Thomas Brox. U-net: Convolutional networks for biomedical image segmentation. In *Medical Image Computing and Computer-Assisted Intervention—MICCAI 2015: 18th International Conference, Munich, Germany, October 5-9, 2015, Proceedings, Part III 18*, pages 234–241. Springer, 2015.
- [28] Fabian Isensee, Paul F Jaeger, Simon AA Kohl, Jens Petersen, and Klaus H Maier-Hein. nnu-net: a self-configuring method for deep learning-based biomedical image segmentation. *Nature methods*, 18(2):203–211, 2021.
- [29] Jieneng Chen, Yongyi Lu, Qihang Yu, Xiangde Luo, Ehsan Adeli, Yan Wang, Le Lu, Alan L Yuille, and Yuyin Zhou. Transunet: Transformers make strong encoders for medical image segmentation. *arXiv preprint arXiv:2102.04306*, 2021.
- [30] Ziheng Zhao, Yao Zhang, Chaoyi Wu, Xiaoman Zhang, Ya Zhang, Yanfeng Wang, and Weidi Xie. One model to rule them all: Towards universal segmentation for medical images with text prompt. *arXiv preprint arXiv:2312.17183*, 2023.
- [31] Ting Chen, Saurabh Saxena, Lala Li, David J Fleet, and Geoffrey Hinton. Pix2seq: A language modeling framework for object detection. *arXiv preprint arXiv:2109.10852*, 2021.
- [32] Ting Chen, Saurabh Saxena, Lala Li, Tsung-Yi Lin, David J Fleet, and Geoffrey E Hinton. A unified sequence interface for vision tasks. *Advances in Neural Information Processing Systems*, 35:31333–31346, 2022.

- [33] Jiasen Lu, Christopher Clark, Rowan Zellers, Roozbeh Mottaghi, and Aniruddha Kembhavi. Unified-io: A unified model for vision, language, and multi-modal tasks. *arXiv preprint arXiv:2206.08916*, 2022.
- [34] Peng Wang, An Yang, Rui Men, Junyang Lin, Shuai Bai, Zhikang Li, Jianxin Ma, Chang Zhou, Jingren Zhou, and Hongxia Yang. Ofa: Unifying architectures, tasks, and modalities through a simple sequence-to-sequence learning framework. In *International Conference on Machine Learning*, pages 23318–23340. PMLR, 2022.
- [35] Tom B Brown, Benjamin Mann, Nick Ryder, Melanie Subbiah, Jared Kaplan, Prafulla Dhariwal, Arvind Neelakantan, Pranav Shyam, Girish Sastry, Amanda Askell, et al. Language models are few-shot learners. *preprint arXiv:2005.14165*, 2020.
- [36] Jean-Baptiste Alayrac, Jeff Donahue, Pauline Luc, Antoine Miech, Iain Barr, Yana Hasson, Karel Lenc, Arthur Mensch, Katherine Millican, Malcolm Reynolds, et al. Flamingo: a visual language model for few-shot learning. *Advances in Neural Information Processing Systems*, 35:23716–23736, 2022.
- [37] Andrew Jaegle, Sebastian Borgeaud, Jean-Baptiste Alayrac, Carl Doersch, Catalin Ionescu, David Ding, Skanda Koppula, Daniel Zoran, Andrew Brock, Evan Shelhamer, et al. Perceiver io: A general architecture for structured inputs & outputs. *arXiv preprint arXiv:2107.14795*, 2021.
- [38] Michael Laskin, Luyu Wang, Junhyuk Oh, Emilio Parisotto, Stephen Spencer, Richie Steigerwald, DJ Strouse, Steven Hansen, Angelos Filos, Ethan Brooks, et al. In-context reinforcement learning with algorithm distillation. *arXiv preprint arXiv:2210.14215*, 2022.
- [39] Jonathan Lee, Annie Xie, Aldo Pacchiano, Yash Chandak, Chelsea Finn, Ofir Nachum, and Emma Brunskill. Supervised pretraining can learn in-context reinforcement learning. *Advances in Neural Information Processing Systems*, 36, 2024.
- [40] Florian Kofler, Felix Meissen, Felix Steinbauer, Robert Graf, Eva Oswald, Ezequiel de da Rosa, Hongwei Bran Li, Ujjwal Baid, Florian Hoelzl, Oezguen Turgut, et al. The brain tumor segmentation (brats) challenge 2023: Local synthesis of healthy brain tissue via inpainting. *arXiv preprint arXiv:2305.08992*, 2023.
- [41] Bennett Landman, Zhoubing Xu, J Igelsias, Martin Styner, T Langerak, and Arno Klein. Miccai multi-atlas labeling beyond the cranial vault—workshop and challenge. In *Proc. MICCAI Multi-Atlas Labeling Beyond Cranial Vault—Workshop Challenge*, volume 5, page 12, 2015.
- [42] Kaiming He, Xinlei Chen, Saining Xie, Yanghao Li, Piotr Dollár, and Ross Girshick. Masked autoencoders are scalable vision learners. In *CVPR*, 2022.
- [43] Mark Chen, Alec Radford, Rewon Child, Jeffrey Wu, Heewoo Jun, David Luan, and Ilya Sutskever. Generative pretraining from pixels. In Hal Daumé III and Aarti Singh, editors, *Proceedings of the 37th International Conference on Machine Learning*, volume 119 of *Proceedings of Machine Learning Research*, pages 1691–1703. PMLR, 13–18 Jul 2020.
- [44] Tianyu Hua, Yonglong Tian, Sucheng Ren, Michalis Raptis, Hang Zhao, and Leonid Sigal. Self-supervision through random segments with autoregressive coding (randsac). In *The Eleventh International Conference on Learning Representations*, 2022.
- [45] Alexey Dosovitskiy, Lucas Beyer, Alexander Kolesnikov, Dirk Weissenborn, Xiaohua Zhai, Thomas Unterthiner, Mostafa Dehghani, Matthias Minderer, Georg Heigold, Sylvain Gelly, et al. An image is worth 16x16 words: Transformers for image recognition at scale. *preprint arXiv:2010.11929*, 2020.
- [46] Yanghao Li, Hanzi Mao, Ross Girshick, and Kaiming He. Exploring plain vision transformer backbones for object detection. In *European Conference on Computer Vision*, pages 280–296. Springer, 2022.
- [47] Juan Eugenio Iglesias and Mert R Sabuncu. Multi-atlas segmentation of biomedical images: a survey. *Medical image analysis*, 24(1):205–219, 2015.
- [48] Hongxu Jiang, Muhammad Imran, Preethika Muralidharan, Anjali Patel, Jake Pensa, Muxuan Liang, Tarik Benidir, Joseph R Grajo, Jason P Joseph, Russell Terry, et al. Microsegnet: a deep learning approach for prostate segmentation on micro-ultrasound images. *Computerized Medical Imaging and Graphics*, 112:102326, 2024.

- [49] Geert Litjens, Robert Toth, Wendy van de Ven, Caroline Hoeks, Sjoerd Kerkstra, Bram van Ginneken, Graham Vincent, Gwenael Guillard, Neil Birbeck, Jindang Zhang, et al. Evaluation of prostate segmentation algorithms for mri: the promise12 challenge. *Medical image analysis*, 18(2):359–373, 2014.
- [50] Anahita Fathi Kazerooni, Nastaran Khalili, Xinyang Liu, Debanjan Haldar, Zhifan Jiang, Syed Muhammed Anwar, Jake Albrecht, Maruf Adewole, Udunna Anazodo, Hannah Anderson, et al. The brain tumor segmentation (brats) challenge 2023: Focus on pediatrics (cbtn-connect-dipgr-asnr-miccai brats-peds). *ArXiv*, 2023.
- [51] C McCollough, B Chen, D Holmes, X Duan, Z Yu, L Xu, S Leng, and J Fletcher. Low dose ct image and projection data (ldct-and-projection-data)(version 4). *Med. Phys*, 48:902–911, 2021.
- [52] Sema Candemir and Sameer Antani. A review on lung boundary detection in chest x-rays. *International journal of computer assisted radiology and surgery*, 14:563–576, 2019.
- [53] Olivier Bernard, Alain Lalande, Clément Zotti, Frédéric Cervenansky, Xin Yang, et al. Deep learning techniques for automatic mri cardiac multi-structures segmentation and diagnosis: Is the problem solved? *IEEE Transactions on Medical Imaging*, 37:2514–2525, 2018.
- [54] Chen Chen, Wenjia Bai, and Daniel Rueckert. Multi-task learning for left atrial segmentation on ge-mri. In *Statistical Atlases and Computational Models of the Heart. Atrial Segmentation and LV Quantification Challenges: 9th International Workshop, STACOM 2018, Held in Conjunction with MICCAI 2018, Granada, Spain, September 16, 2018, Revised Selected Papers 9*, pages 292–301. Springer, 2019.
- [55] Michela Antonelli, Annika Reinke, Spyridon Bakas, Keyvan Farahani, Annette Kopp-Schneider, Bennett A Landman, Geert Litjens, Bjoern Menze, Olaf Ronneberger, Ronald M Summers, et al. The medical segmentation decathlon. *Nature communications*, 13(1):4128, 2022.
- [56] Kaiming He, Xiangyu Zhang, Shaoqing Ren, and Jian Sun. Deep residual learning for image recognition. In *CVPR*, 2016.
- [57] Fausto Milletari, Nassir Navab, and Seyed-Ahmad Ahmadi. V-net: Fully convolutional neural networks for volumetric medical image segmentation. In *2016 fourth international conference on 3D vision (3DV)*, pages 565–571. Ieee, 2016.
- [58] Phillip Isola, Jun-Yan Zhu, Tinghui Zhou, and Alexei A Efros. Image-to-image translation with conditional adversarial networks. In *Proceedings of the IEEE conference on computer vision and pattern recognition*, pages 1125–1134, 2017.

## A Visualization

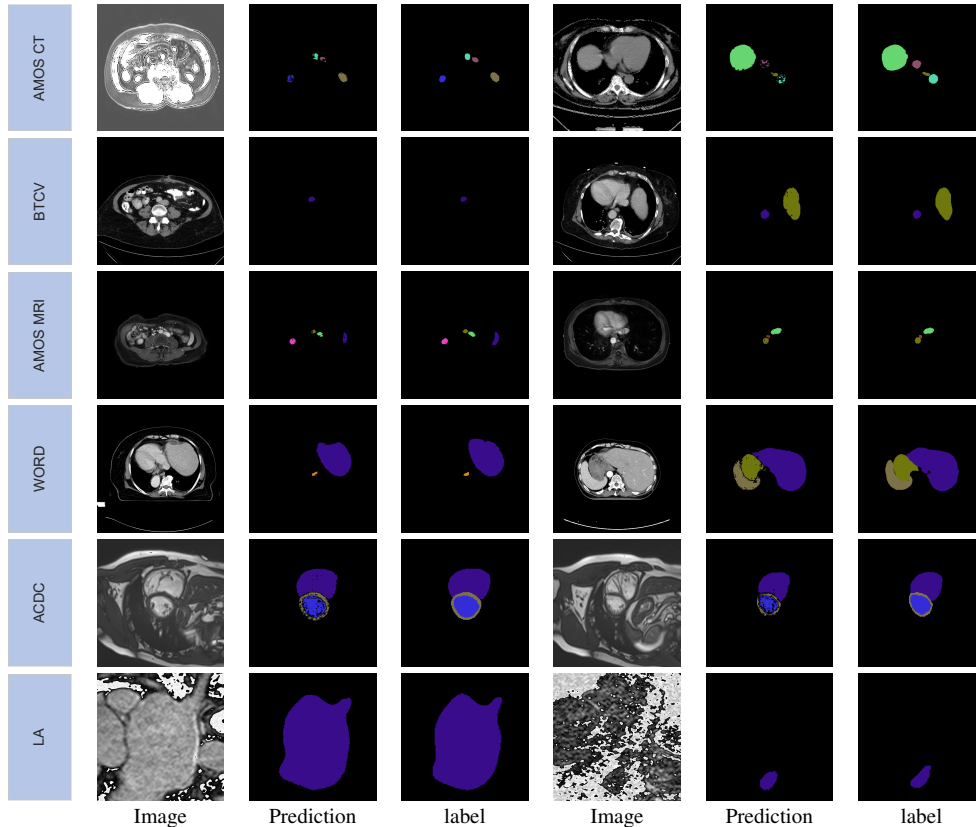


Figure 6: **Qualitative evaluation of segmentation.** MVG shows strong capabilities on various segmentation tasks covering multiple modalities and body regions.

In the paper, we only visualize one segmentation dataset. Here, we provide visualization results on more segmentation datasets as shown in Figure 6.

Method	AMOS CT	WORD	BTCV	AMOS MRI	MicroSegNet	PROMISE	Chest Defect	ACDC	LA
Sup.	0.55	0.57	0.57	0.58	0.80	0.70	0.68	0.69	0.68
Natural MIM	0.69	0.70	0.68	0.69	0.89	0.83	0.76	0.81	0.78
Medical MIM	0.73	0.74	0.73	0.74	0.91	0.85	0.79	0.85	0.81

Table 6: **Pre-training on medical data is important.** We initialize the encoder with natural image supervised pretrained model, natural image mask image modeling pretrained model, and medical image mask image modeling pretrained model.

## B Pretraining

Most parameters of our medical vision generalist are from the ViT encoder. Recent works prove that pretraining makes ViT learn more robust and transferable representations. Traditionally, the supervised pretrained model [29] on ImageNet is loaded as the model initialization for various medical segmentation tasks (Sup.). Recent progress in self-supervised learning demonstrates that the model pretrained by mask image modeling achieves better generalization. Therefore, for comparison, we load the MAE, which trains the model on a natural image for comparison (Natural MIM). However, the domain gap between natural images and medical images limits the power of medical vision tasks. Therefore, we train a model with mask image modeling on medical images for comparison. As shown in Table 6, the superiority of the Medical MIM approach is evident, with the model achieving the highest performance metrics across all evaluated tasks

## **C Societal Impact**

MVG promises to adapt to new medical imaging tasks easily, given in-context samples that represent the new tasks. We believe MVG can serve as a stepstone to make medical imaging tools more accessible to clinical researchers, other scientists, or beyond, by lowering the bar of machine learning expertise, computational resources, and human labor. Since our method is data-driven, the bias in the data would be inherited by models. The users should be aware of the bias and its potential detriment.